Adaptive Threshold Adjustment Strategy Based on Fuzzy Logic Control for Ground Energy Storage System in Urban Rail Transit

Yuyan Liu, *Student Member, IEEE*, Zhongping Yang, *Member, IEEE*, Xiaobo Wu, *Member, IEEE*, Lifu Lan, *Student Member, IEEE*, Fei Lin, *Member, IEEE*, Hu Su, *Member, IEEE*, and Jiangbo Huang, *Member, IEEE*

***Abstract*—The installation of a ground energy storage system (ESS) in the substation can improve the recovery and utilization of regenerative braking energy. This paper proposes an energy management strategy (EMS) of adaptive threshold adjustment for ground ESS. In this regard, this paper analyzes the energy flow in traction power supply system (TPSS) with different headways and no-load voltage. According to the influence of charge and discharge threshold on the energy flow in TPSS, the laws of energy flow are formulated. Subsequently, an EMS based on fuzzy logic control (FLC) is designed. The proposed EMS is adaptive to the variation of headway and no-load voltage. By monitoring the charge-discharge effect of ESS and the variation of substation output energy within two adjacent periods, the charge-discharge threshold is adjusted adaptively to guarantee the recovery effect of regenerative braking energy. Finally, the simulation and field experiment of proposed EMS are carried out with ground energy storage device and actual line conditions of Beijing Batong line. The experiment results indicate the good performance of proposed EMS in terms of energy saving.**

***Index Terms*—Energy storage system (ESS), energy management strategy, fuzzy logic control, energy saving.**

NOMENCLATURE

U_{sub}	DC voltage of the substation
U_{d0}, U_{d1}	Equivalent voltage of substation
I_{sub}	Substation current
R_{eq0}, R_{eq1}	Equivalent resistance of substation
I_g	Critical current
U_{char}	Charge voltage threshold of SC
U_{dis}	Discharge voltage threshold of SC
ΔU_{char}	Adjustment of charge threshold
ΔU_{dis}	Adjustment of discharge threshold
$U_{sc\cdot max}$	Maximum/minimum voltage of SC
$U_{sc\cdot min}$	Maximum/minimum voltage of SC
$E_{exchange}$	Energy interaction between the trains
E_{bra_res}	Consumed energy by on-board brake resistance
$P_{train.i}$	Traction power of train *i*
$P_{sub.j}$	Output power of substation *j*
$P_{bra.i}$	Power consumed by brake resistance of train *i*
E_{tra}	Traction energy of trains
E_{bra}	Brake energy of the trains
E_{sub}	Output energy of substation
$E_{sc\cdot in}$	Charge energy of SC
$E_{sc\cdot out}$	Discharge energy of SC
T_h	Headway
U_o	No-load voltage of substation
J_1	Energy saving rate
J_2	Train energy interaction ratio
ΔE_{sub}	Variation of substation output energy
$\Delta E_{sc\cdot in}$	Variation of SC charge energy
$\Delta E_{sc\cdot out}$	Variation of SC discharge energy
U_1	Trigger Voltage of on-board brake resistance

Manuscript received July 2, 2021; revised August 30, 2021; accepted August 31, 2021. Date of publication September 2, 2021; date of current version October 15, 2021. This work was supported by the National Innovation Center of High Speed Train (Qingdao). The review of this article was coordinated by Dr. Zhigang Liu. *(Corresponding author: Fei Lin.)*

Yuyan Liu, Zhongping Yang, Lifu Lan, Fei Lin, and Hu Su are with the School of Electrical Engineering, Beijing Jiaotong University, Beijing 100044, China (e-mail: 18117014@bjtu.edu.cn; zhpyang@bjtu.edu.cn; 19121442@bjtu.edu.cn; flin@bjtu.edu.cn; hsun1@bjtu.edu.cn).

Xiaobo Wu is with the National Innovation Center of High Speed Train, Qingdao 266111, China (e-mail: wuxiaobo@innohst.com).

Jiangbo Huang is with the School of Robot Engineering, Yangtze Normal University, Chongqing 408100, China (e-mail: 19990002@yznu.edu.cn).

Digital Object Identifier 10.1109/TVT.2021.3109747

I. INTRODUCTION

WITH the rapid development of urban rail transit system, the operation energy consumption increases greatly. Reducing the energy consumption of urban rail transit is of great significance to the whole society in energy conservation and emission reduction. The regenerative braking energy of the train in the urban rail transit system is considerable [1]–[3], and the utilization of the energy storage system (ESS) can effectively recover and reuse the regenerative braking energy. ESS can be divided into on-board and ground. The use of on-board ESS would be limited by the volume and weight, and the installation of ESS on each train increases the investment cost. Obviously, the ground ESS has advantages in these two aspects [4]. In the urban rail transit system, the ESS mainly plays the roles of voltage compensation, power peak reduction, recovery of regenerative braking energy and emergency traction [5]–[8].

At present, the control of ground ESS in the existing literature mainly includes voltage based, ESS state based, train operation state based and intelligent optimization algorithm based.

Literatures [9]–[10] control the charge and discharge of the ESS based on line voltage. However, the catenary voltage is also fluctuated by the influence of utility grid, so the no-load voltage of the substation is not a constant value. The value of no-load voltage can be obtained through the catenary voltage at 10kV side [11], but the voltage at 10kV side would also be affected by the side of DC 750 V. Some added 5th harmonic voltage tests to judge the traction load level on the line [12]. It can also fit the external characteristic curve of the substation according to the historical data, and identify the no-load voltage value through the real-time voltage and current of the substation [13]. Because the voltage of substation fluctuates in real time when the train is running, it is difficult to get the accurate no-load voltage value through the method in [11]–[13].

The control strategies based on charge and discharge threshold can effectively recover regenerative braking energy and reduce voltage drop [14],[15]. In [16], the state machine is used to control the charge and discharge of ESS by detecting the line voltage. The control strategy proposed in [17] considers energy conversion efficiency, and calculates the reference voltage value of Li-ion capacitor based on train kinetic energy to compensate voltage and reduce current peak. Considering the complexity of the energy flow in the TPSS, only tracking the charge and discharge state of the ESS cannot reflect the recovery effect of regenerative braking energy. In [18], the voltage and current of ESS can be evaluated in real time according to the kinetic energy of the train. The time-varying part related to the train was ignored for simplifying reference voltage value. The proposed strategy in [19] considers the operation status of substation, ESS and on-board brake resistance, so as to establish energy management state machine to maximize the utilization of ESS by monitoring line voltage and train status. These methods can improve the recovery of regenerative braking energy by taking into account the state information of train, but they are difficult to meet the needs of multiple trains operation between substations.

In [20], the optimal reference voltage value of ESS is solved by using the classical algorithm of variational calculus with the aim of minimizing the line loss, which is related to the power and position of the train. Literature [21] proposed an operation optimization strategy of hybrid energy storage system based on dynamic programming. However, as the topology of traction power supply system changes in real time, dynamic programming cannot realize online optimal control. In [22], train operation scenarios are classified based on timetable and train operation laws, and the capacity of ESS is reasonably allocated with the optimization goal of minimizing total energy consumption and voltage drop to realize the online control of SC. At present, there are also many studies [23]–[26] on the adaptive control strategy of the ground ESS. An optimization strategy proposed in [23] is based on the linearization of DC load flow equation, and uses successive approximation method to obtain the reference value of the charge and discharge threshold of ESS. To maximize the energy saving rate and the voltage stabilizing rate, the online control of ESS based on deep reinforcement learning has been studied in [24]–[26]. However, most of adaptive EMSs need to get the real-time information of train, which requires high information transmission rate and accuracy between train and ground ESS.

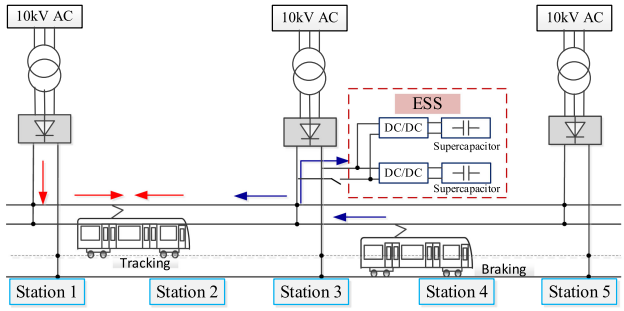

Fig. 1. The structure of traction power supply system.

Fuzzy logic control (FLC) can realize the real-time control of ESS in the TPSS with time-varying nonlinearity. At present, FLC method has been widely used in electric vehicles due to its intelligent characteristics and realizability. In [27], FLC based on cyclic optimization membership function is proposed to prolong the battery life of vehicle, so that the control effect is close to the optimal result of dynamic programming. Some studies use FLC to realize the reasonable distribution of sources within the vehicle [28]–[32]. To realize real-time optimal power distribution of hybrid energy storage system, the FLC was used to track the battery state of charge (SOC) curve which trained by the neural network [33]. In this paper, the energy distribution of TPSS is analyzed, and the correspondence among no-load voltage variation, headway variation and ESS charge/discharge energy, substation output energy is extracted. According the extracted correspondence, an EMS for ground ESS based on FLC is proposed. It adjusts charge/discharge threshold adaptively to increase the energy interaction between trains and improve the utilization of regenerative energy.

This work is organized as follows: In Section II, the model of TPSS with ground ESS is established. In Section III, the energy distribution of TPSS is extracted by simulation. The EMS of ESS based on FLC is proposed in Section IV. In Section V, the EMS of ground ESS is simulated and verified based on the data of Batong line. In Section VI, the ground ESS device is used to verify the proposed strategy in Liyuan station of Beijing Batong Line. Section VII is the summary.

II. Modeling of The TPSS With ESS

For the purpose of this manuscript, a model of TPSS is build, as shown in Fig. 1. A TPSS model including three substations, a set of ground ESS and a multi-train running between five stations is constructed. In this work, the mathematical model of TPSS is established. Then the energy distribution in the TPSS is analyzed, as well as the relationship between the control parameters of ESS and the load characteristics of the TPSS.

A. System Model

In this system, there involve three types of energy source,1) substations, 2) ESS, 3) trains.

1) Substations: Two 12-pulse rectifying units of AC10kV/DC750 V in the traction substation are equivalent to 24-pulse rectifying and output DC750 V electric energy to supply power to the TPSS. The equivalent model of substation

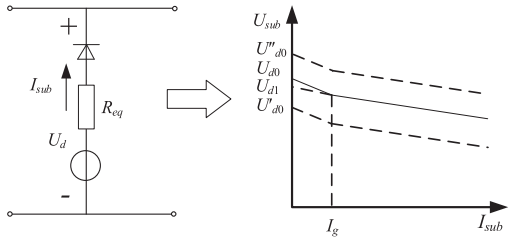

Fig. 2. No-load voltage output characteristic.

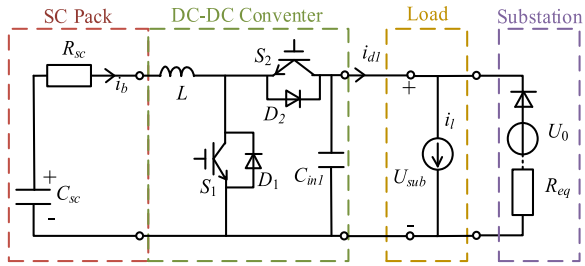

Fig. 3. The structure of ESS.

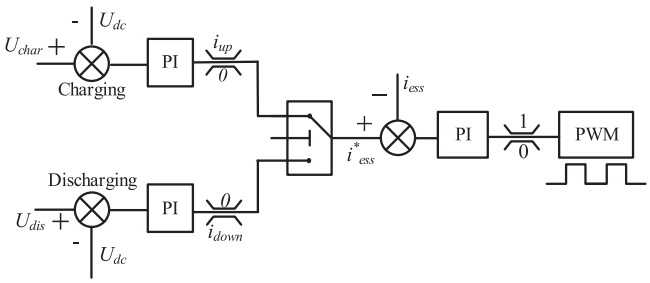

Fig. 4. ESS control strategy schematic.

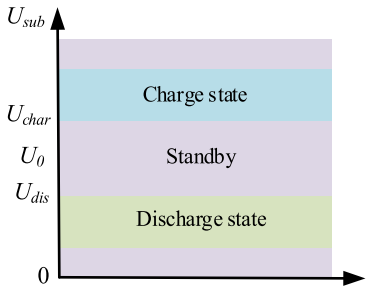

Fig. 5. Traction substation voltage control strategy.

can be replaced by an ideal voltage source and equivalent internal resistance in series [11]. The output characteristic of substation is shown in the Fig. 2 and it can be expressed as

$$U_{sub} = \begin{cases} U_{d0} - I_{sub} \cdot R_{eq0} & 0 < I_{sub} < I_g \\ U_{d1} - I_{sub} \cdot R_{eq1} & I_g < I_{sub} \end{cases} \quad (1)$$

2) ESS: ESS is installed in the substation. The ESS consists of bi-directional DC /DC converter and SC packs, as shown in Fig. 3. The controller of ESS determines whether it is charge and discharge according to U_{sub}, as shown in Fig. 4 and Fig. 5. Where U_{sub} exceeds the charge threshold U_{char}, ESS switches to the charge state. When U_{sub} below the discharge threshold U_{dis},

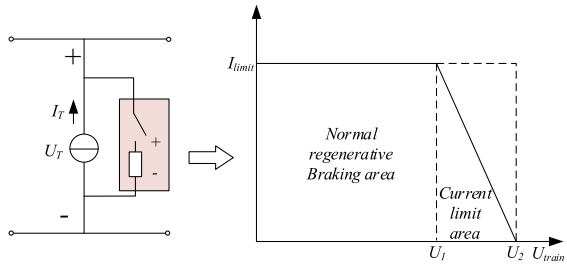

Fig. 6. Characteristic curve of onboard brake resistance.

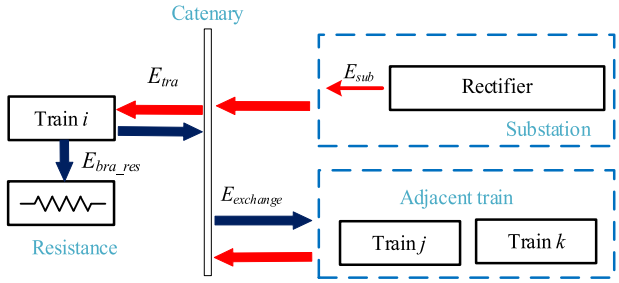

Fig. 7. Diagram of energy flow for TPSS without ESS.

ESS switches to the discharge state. When the U_{sub} is between U_{char} and U_{dis}, the ESS is in standby mode. In addition, the voltage of SC is also constrained, SC stops working when the voltage of SC is greater than $U_{sc\cdot max}$ or less than $U_{sc\cdot min}$, and its can be expressed as

$$U_{sc\_\min} < U_{sc} < U_{sc\_\max} \quad (2)$$

The supercapacitor SOC [33] expression is shown below

$$SOC_{SC} = U^2_{SC}/U^2_{SC\_\max} \quad (3)$$

3) Train: During the train traction process, the traction substation, the adjacent braking train and ESS provide power to the trains and the voltage of pantograph drops. During the train braking process, the train generates regenerative braking energy that feeds back to the dc grid, making the voltage of pantograph increases. Considering the limiting characteristics of the regenerative braking current, while the dc voltage exceeds the allowable range, the on-board braking resistance is connected to limit the increase of dc voltage of catenary. The train model is shown in Fig. 6. The train can be replaced by a controlled current source. When the train is braking, the on-board brake resistor adjusts the on/off of the brake chopper according to the voltage of the filter capacitor on the dc side of the traction converter, and changes its equivalent resistance to consume regenerative braking energy.

B. Energy Distribution Description of TPSS

The energy flow diagrams of the traction power supply system without ground ESS and with ground ESS are shown in Fig. 7 and Fig. 8, respectively. The traction energy of the train E_{tra}, the brake energy of the train E_{bra} and the output energy of the

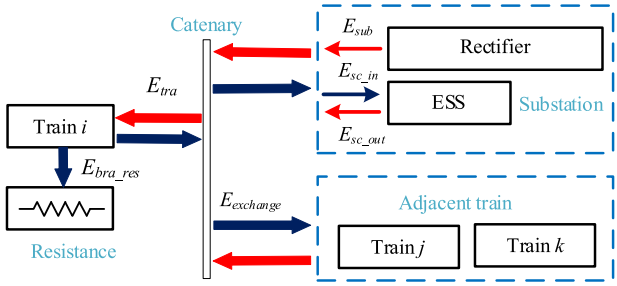

Fig. 8 Diagram of energy flow for TPSS with ESS.

traction substation E_{sub} can be expressed as

$$E_{tra} = \sum_{i=1}^{n} \int_0^T P_{train.i} dt \ , \ if \ P_{train.i} > 0 \tag{4}$$

$$E_{bra} = \sum_{i=1}^{n} \int_0^T P_{train.i} dt \ , \ if \ P_{train.i} < 0 \tag{5}$$

$$E_{sub} = \sum_{j=1}^{3} \int_0^T P_{sub.j} dt \tag{6}$$

In Fig. 7, the regenerative braking energy of the train can only be used by $E_{exchange}$ and consumed by E_{bra_res}. Because the line resistance is small [8], the influence of the line resistance loss is ignored in this paper. Meanwhile, the energy consumed by the braking resistance E_{bra_res} and the interactive energy between the trains $E_{exchange1}$ are formulated as

$$\begin{cases} E_{bra\_res} = \sum_{i=1}^{n} \int_0^T P_{bra.i} dt \\ E_{exchange} = E_{bra} - E_{bra\_res} \end{cases} \tag{7}$$

In Fig. 8, E_{tra} required by train i comes from the TPSS (E_{sub}), ESS (E_{sc_out}) and the adjacent brake trains ($E_{exchange}$). Part of the regenerative braking energy generated by train i can be absorbed by the nearby traction trains, and the rest of the regenerative braking energy can be stored by ESS (E_{sc_in}) or consumed by the on-board brake resistance (E_{bra_res}). The energy distribution in the TPSS with ESS can be expressed as

$$\begin{cases} E_{sc\_in} = \int_0^T P_{sc} dt \ , \ if \ P_{sc} > 0 \\ E_{sc\_out} = \int_0^T P_{sc} dt \ , \ if \ P_{sc} < 0 \\ E_{exchange} = E_{bra} - E_{bra\_res} - E_{sc\_in} \end{cases} \tag{8}$$

In order to improve the energy saving rate [9], it is necessary to establish a quantifiable evaluation index J_1. At the same time, in order to ensure the direct utilization of regenerative energy in the catenary, this paper also needs to establish J_2 to evaluate the direct utilization of regenerative energy.

$$J_1 = \left(1 - \frac{E_{sub\_sc}}{E_{sub\_nosc}}\right) \times 100\% \tag{9}$$

$$J_2 = \frac{E_{exchange}}{E_{bra}} \times 100\% \tag{10}$$

TABLE I
PARAMETERS OF LINE

Station	Guoyuan	Jiukeshu	Liyuan	Linheli	Tuqiao
Location (m)	0	990	2215	3472	4249

TABLE II
PARAMETERS OF TRAIN

Parameter	Value
Train formation	3M3T
Inverter efficiency	0.86
Gear efficiency	0.975
Motor efficiency	0.92
Auxiliary power	160KVA*2
weight	303t

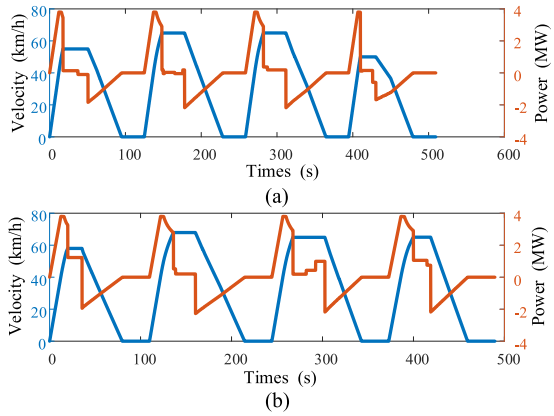

Fig. 9. The running curve of the train (a) up line (b) down line.

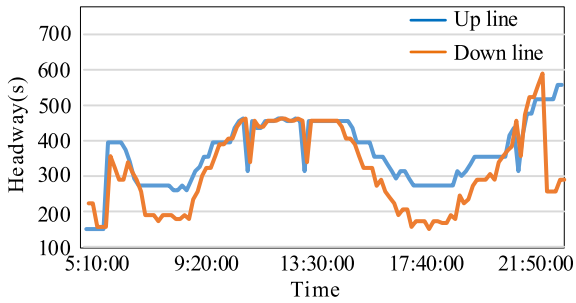

Fig. 10. Headway of the trains on a day of Batong line.

III. ENERGY DISTRIBUTION LAWS OF TPSS

In this work, take Guoyuan station to Tuqiao station of Beijing Batong Line for example to carry out the following analysis about energy distribution laws of TPSS. Line conditions are shown in Table I. The whole length of the simulated line is 4249m. Train parameters are shown in Table II, and the operation curve of train is shown in Fig. 9.

Fig. 10 shows the headway of the trains on a day of Beijing Batong line. It can be seen that the headway varies between 150 s and 600 s. Fig. 11 is a schematic diagram of the train operation

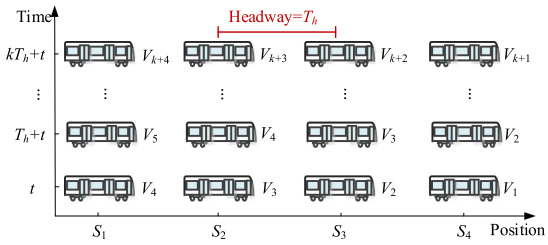

Fig. 11. The schematic diagram of the train operation process on the line.

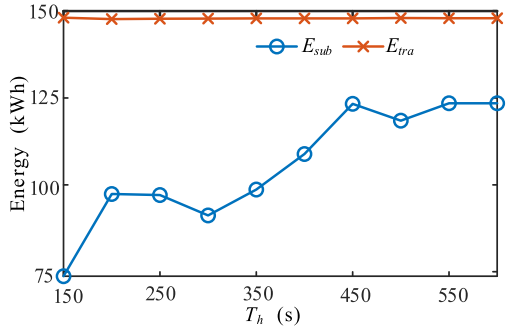

Fig. 12. Output energy of substation and traction energy of trains at different headways.

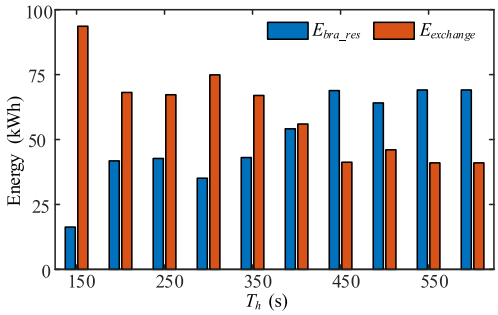

Fig. 13. Distribution of regenerative braking energy that feeds back to the catenary at different headways.

process on the line. It is assumed that the train on the line adopts automatic operation. The operation process of the trains on the line take the T_h as a cycle, so the subsequent work takes T_h as a cycle for analysis.

A. Without ESS

The headway is one of the important factors affecting the energy interaction between trains. The output energy of substation and the consume energy of on-board braking resistance vary with the headway [8],[24]. Take the headway as the simulation period, the relationship between the output energy of substation and the headway without ESS is shown in Fig. 12. With the increase of headway, the energy interaction between trains decreases, the output energy of traction substation E_{sub} increases. The interactive energy ($E_{exchange}$) and on-board brake resistance energy consumption of trains (E_{bra_res}) at different headway without ESS are shown in the Fig. 13. It can be seen that with a rise of headway, $E_{exchange}$ decreases and E_{bra_res} is becoming larger.

TABLE III
PARAMETERS OF ESS

Type	Rated voltage	i_{max}	Capacitance
SC	672V	1600A	97.3F

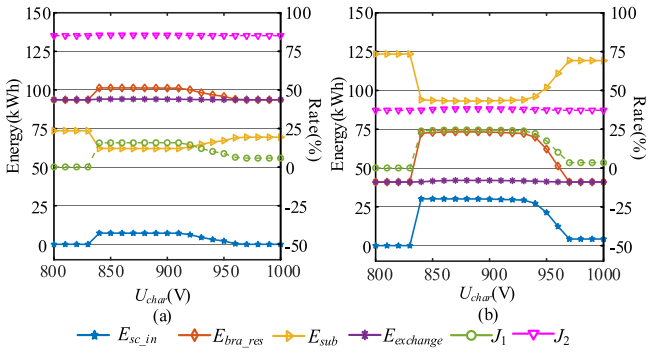

Fig. 14. The relationship between energy distribution of TPSS and charge voltage threshold at the no-load voltage of 836 V (a) T_h is 150 s, U_{dis} is 830 V and (b) T_h is 600 s, U_{dis} is 830 V.

B. With ESS

Under the premise of avoiding the on-board brake resistor starting, the setting value of U_{char} should be as high as possible to facilitate the energy interaction between trains. However, when the headway is short and the train departure density is large, the braking power fluctuates greatly. So, the voltage at the pantograph fluctuates significantly when the train braking, and the larger charge threshold would make the regenerated energy be consumed by the on-board braking resistance in priority. Therefore, in order to prevent regenerative braking energy from being absorbed by the on-board braking resistance in priority, the maximum U_{char} of the short headway should be less than that of the long headway. In addition, fluctuations in the no-load voltage may also cause ESS to be unable to charge or discharge.

In order to analyze the effect of U_{char} and U_{dis} on regenerative braking energy recovery and energy interaction between trains, the energy flow distribution of TPSS with ESS would be analyzed considering the fluctuations of headway and no-load voltage in this section. Taking ground ESS installed in Liyuan Station as an example, the influence of charge/discharge threshold on the energy flow of TPSS is analyzed. The parameters of ESS are shown in Table III.

Fig. 14 illustrates the influence of the variation of U_{char} on the energy flow of TPSS under the headways of 150 s and 600 s. When the headway is 600 s, compared with the headway of 150 s, the charge energy of ESS increases and the output energy of the substation also increases. Fig. 14 shows that the ESS cannot be charged when the charge threshold is less than 830 V. Since the U_{char} is less than U_{dis}, the ESS cannot charge. It can be known from Fig. 14(a) that when U_{char} is greater than 910 V, J_1 drops significantly under the headway of 150 s. Fig. 14(b) exhibits that when U_{char} is greater than 930 V, J_1 drops significantly under the headway of 600 s.

Fig. 15 compares TPSS energy distribution under different no-load voltages. From Fig. 15, the higher the no-load voltage,

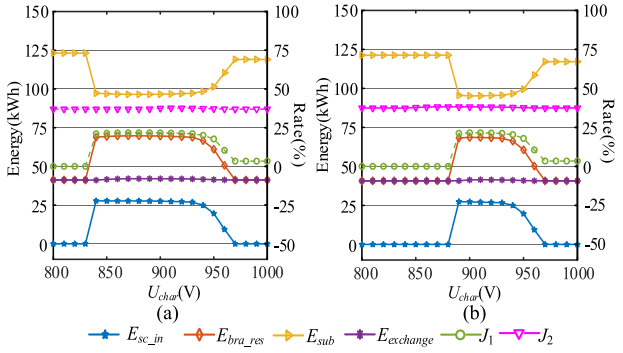

Fig. 15. The relationship between energy distribution of TPSS and charge voltage threshold at the T_h of 450 s (a) U_0 is 836 V, U_{dis} is 830 V and (b) U_0 is 890 V, U_{dis} is 880 V.

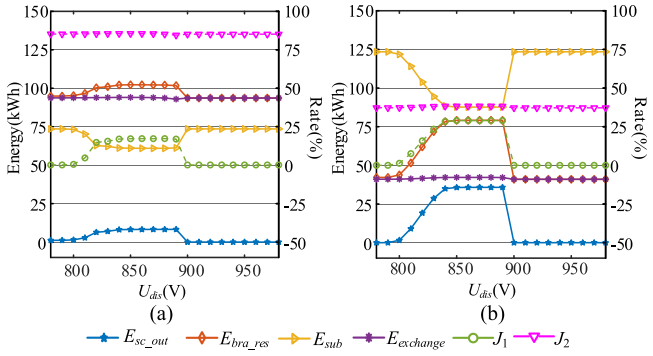

Fig. 16. The relationship between energy distribution of TPSS and discharge voltage threshold at the no-load voltage of 836 V (a) T_h is 150 s, U_{char} is 890 V and (b) T_h is 600 s, U_{char} is 890 V.

the smaller U_{char} setting range that can make ESS recover regenerative braking energy. Take U_{char} as 870 V for example, while U_0 is 836 V shown in Fig. 15(a), the ESS has a good charge performance. However, while the no-load voltage is 886 V, E_{sc_in} would be reduced to 0, and the output energy of the substation would increase from the original 98.4 kWh to 123.1 kWh shown in Fig. 15(b). In this case, the charge threshold of the ESS should be increased. to improve regenerative braking energy recovery.

Similarly, in order to characterize the influence of ESS discharge voltage threshold on TPSS, the variation trend of substation output energy and ESS discharge energy is used to describe. Fig. 16 illustrates the influence of the variation of U_{dis} under the headways of 150 s and 600 s. Since U_{dis} does not affect the starting of the on-board brake resistance, when the headway changes, the reasonable setting range of U_{dis} remains basically unchanged which shown in Fig. 16. Therefore, when the headway changes, if the discharge energy is reasonable, there is no need to adjust the U_{dis}. Fig. 17 shows TPSS energy distribution under different no-load voltages. Fig. 17 presents that the E_{sc_out} is 28.7 kWh when the discharge threshold of the ESS is 840 V under the no-load voltage of 836 V. Under the discharge threshold of 840 V, while the no-load voltage is 890 V, E_{sc_out} is reduced to 0 kWh. In this case, the discharge threshold needs to be raised to improve J_1.

Table IV illustrates the complete correspondence between U_0/T_h state and energy state. The symbol '↑', '↓' and '—'

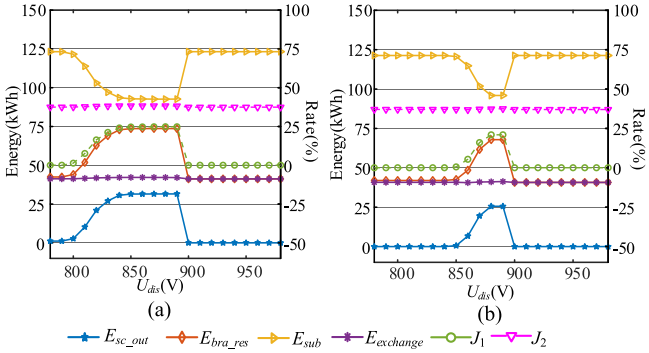

Fig. 17. The relationship between energy distribution of TPSS and discharge voltage threshold at the T_h of 450 s (a) U_0 is 836 V, U_{char} is 890 V and (b) U_0 is 886 V, U_{char} is 890 V.

TABLE IV
TABLE OF RELATIONSHIPS BETWEEN STATE CHANGES AND CORRESPONDING ENERGY PHENOMENA

State	E_{sc_in}	E_{sc_out}	E_{sub}
U_0↑	↓	↓	↑
	—	—	—
U_0 ↓	—	—	↑
	—	—	—
T_h ↑	↑	↑	↑
T_h ↓	↓	↓	↓

represent increase, decrease and invariant, respectively. The fluctuation of no-load voltage and headway corresponds to the energy variation trend of the substation and ESS is different. The change of U_0 may lead to poor energy saving effect. In the case of E_{sc_in}, E_{sc_out} reduction and E_{sub} increase caused by U_0 increase, U_{char} and U_{dis} need to be changed to restore the energy saving effect of ESS. In the condition that E_{sc_in}, E_{sc_out} remain unchanged and E_{sub} increases due to U_0 reduction, U_{char} and U_{dis} also need to be changed. The change of T_h can lead to the corresponding energy change of ESS and substation. At this time, reasonable adjustment of U_{char} and U_{dis} can improve the energy interaction rate between trains.

In other word, while the variation of U_0 and T_h make the energy saving effect worse, the three energy values in Table IV would change, so U_{char} and U_{dis} should be adjusted accordingly.

IV. PROPOSED CONTROL STRATEGY FOR THE ESS

Based on the above analysis, the control strategy of ground ESS based on fuzzy logic control is proposed. The control strategy has the following characteristics: first, control parameters of ESS can be adjusted adaptively to recovery the regenerative energy while the headway changes or no-load voltage changes. The second is to avoid reducing the energy interaction between trains by adjusting threshold.

A. FLC Strategy Framework

The control strategy framework of ESS is designed which shown in Fig. 18. The control structure is divided into two layers,

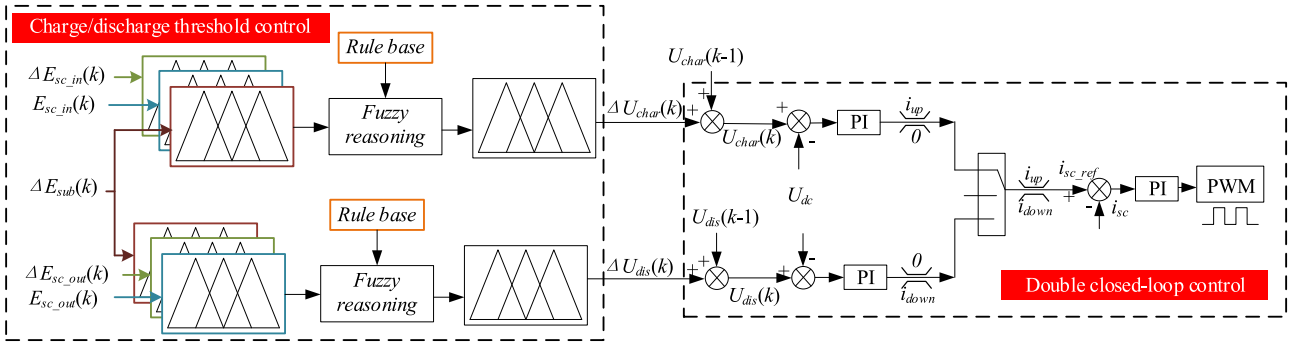

Fig. 18. The control strategy framework of ESS.

the upper layer is charge/discharge threshold control, the lower layer is double closed loop control. In this paper, the threshold adaptive adjustment strategy is proposed for the upper layer. Assuming that the headway between the upper line and down line is the same, each departure time of trains in the platform is taken as the node k. The TPSS energy, ESS charge energy and discharge energy between adjacent nodes k and k-1 would be solved. In proposed control strategy, the charge and discharge energy of ESS and its variation as well as the variation of' substation output energy are taken as inputs, as shown in (11) and (12). The regulation values of charge and discharge voltage threshold for ESS are taken as output values, the charge and discharge voltage threshold of the ESS can be expressed as (13).

$$\begin{cases} \Delta E_{sc\_in}(k) = E_{sc\_in}(k) - E_{sc\_in}(k-1) \\ \Delta E_{sc\_out}(k) = E_{sc\_out}(k) - E_{sc\_out}(k-1) \end{cases} \tag{11}$$

$$\Delta E_{sub}(k) = E_{sub}(k) - E_{sub}(k-1) \tag{12}$$

$$\begin{cases} U_{char}(k) = U_{char}(k-1) + \Delta U_{char}(k) \\ U_{dis}(k) = U_{dis}(k-1) + \Delta U_{dis}(k) \end{cases} \tag{13}$$

In order to ensure the orderliness between U_{char} and U_{dis}, it is necessary to constrain threshold. Moreover, to avoid the U_{char} being higher than the on-board brake resistance start voltage, the following constraint is set.

$$U_{\min} < U_{dis} < U_{char} < U_1 \tag{14}$$

Then, make fuzzy rules based on the above analysis. FLC is good at expressing qualitative knowledge and experience with unclear boundaries. By virtue of the concept of membership function, it can distinguish fuzzy sets, deal with fuzzy relations, and simulate human brain to implement regular reasoning.

B. Membership Functions Design

The performance of the fuzzy logic based EMS is determined by the MF and fuzzy rules. The overall fuzzy logic control is divided into two modules: charge fuzzy logic control and discharge fuzzy logic control. There are three inputs and one output in the designed FLC module. This paper refers to the method of using genetic algorithm to optimize MF proposed in [27]. The MFs in each module are designed as Fig. 19 where the linguistic variables 'VS, M, VB' denote 'very small, medium,

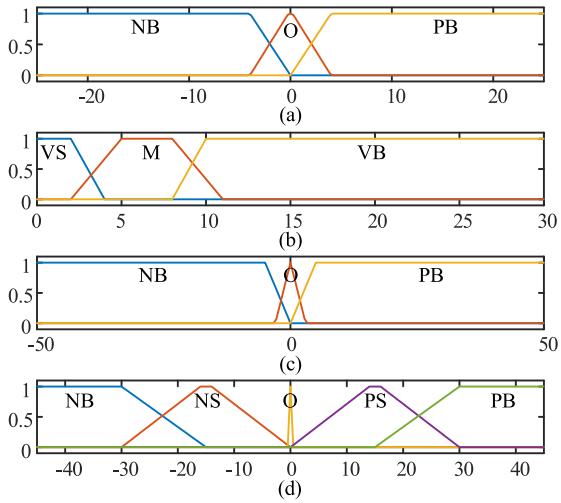

Fig. 19. MFs of (a) $\Delta E_{sc\cdot in}$(kWh) or $\Delta E_{sc\cdot out}$(kWh), (b) $E_{sc\cdot in}$(kWh) or $E_{sc\cdot out}$(kWh), (c) ΔE_{sub}(kWh), and (d) ΔU_{char}(V) or ΔU_{dis}(V).

and very big', and the linguistic variables 'NB, NS, O, PS, PB' denote 'negative big, negative small, zero, positive small and positive big', respectively.

C. Fuzzy Rule of Charge Control Module

According to the principles described in the previous section, while improving the ESS to recover regenerative braking energy, priority should be given to ensuring the energy interaction between trains. The fuzzy rules of charge control module which is shown in Table V are defined as follows. The input-output relational surface of the charge FLC module is shown in Fig. 20.

While $\Delta E_{sc\cdot in}$ is 'NB', shown in Table V the charge energy of ESS is reduced. For example, if $\Delta E_{sc\cdot in}$ is 'NB', $E_{sc\cdot in}$ is 'M', ΔE_{sub} is 'NB' then ΔU_{char} is 'NS'. At this time, compared with the previous cycle, E_{sub} is reduced and the charge energy of the ESS is reduced. The charge energy of the ESS is lower, which is caused by the reduction of the headway. Therefore, the energy interaction between trains can be improved by lowering the charge threshold. If $\Delta E_{sc\cdot in}$ is 'NB', $E_{sc\cdot in}$ is 'S', ΔE_{sub} is 'PB' then ΔU_{char} is 'PB'. At this point, compared with the previous cycle, the output energy of the substation increases and the charge energy of the ESS decrease, while the charge energy

TABLE V
FUZZY RULES OF CHARGE CONTROL

	ΔE_{sub} / ΔE_{sc_in}	NB	O	PB
E_{sc_in} =VS	NB	NS	NS	PB
	O	O	O	NS
	PB	O	O	PS
E_{sc_in} =M	NB	NS	O	PB
	O	O	O	NS
	PB	PS	O	PS
E_{sc_in} =VB	NB	NS	O	PS
	O	O	O	NB
	PB	PS	O	PS

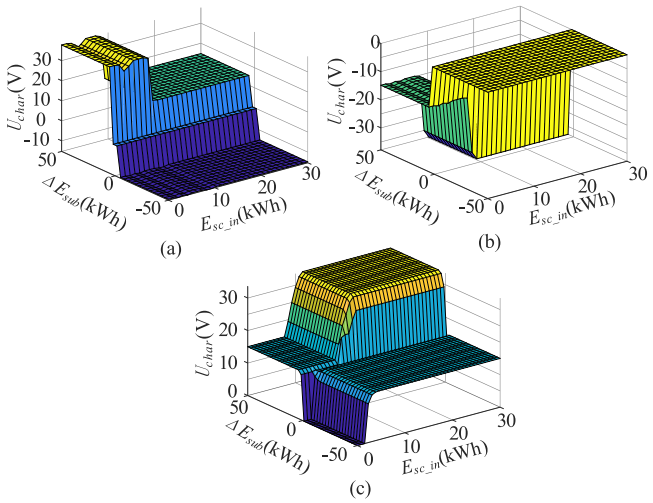

Fig. 20. The input-output relational surface of the charging threshold fuzzy control (a) ΔE_{sc_in} is -25 kWh, (b) ΔE_{sc_in} is 0 kWh, and (c) ΔE_{sc_in} is 25 kWh.

of the ESS is relatively low. This is because ESS cannot discharge due to the raise of no-load voltage. The effect of regenerative energy recovery can be improved by increasing U_{char}. If ΔE_{sub} is 'PB' then ΔU_{char} is 'NB' or 'NS'. The charge energy of the ESS changes little, and the output energy of substation increase. It indicates that the reduction of no-load voltage results in a part of the charge and discharge energy of ESS from the unnecessary supply of the substation, so it is necessary to decrease the U_{char} to reduce unwanted energy supply from substation which is shown in Fig. 20(b).

In the remaining cases which ΔE_{sc_in} is 'O', it can be understood that the charge and discharge energy of ESS does not change. While ΔE_{sc_in} is 'O', there is no need to adjust the threshold.

If ΔE_{sc_in} is 'PB', the increase of E_{sc_in} may be due to the phenomenon that occurs after the headway increases or the U_{char} decreases. Meanwhile, the output energy of the substation is used to judge. When the E_{sub} increases, it can be judged that the headway increases. At this time, the U_{char} can be appropriately raised to increase the energy interaction between trains. While the E_{sub} decreases, the regenerative braking energy can be improved by raising the U_{char}.

TABLE VI
FUZZY RULES OF DISCHARGE CONTROL

	ΔE_{sub} / ΔE_{sc_out}	NB	O	PB
E_{sc_out} =VS	NB	NS	PS	PB
	O	O	PS	NS
	PB	O	O	PS
E_{sc_out} =M	NB	O	O	PS
	O	O	O	NS
	PB	PS	O	PS
E_{sc_out} =VB	NB	O	O	PS
	O	O	O	NB
	PB	PS	O	O

TABLE VII
SIMULATION CONDITIONS IN FOUR CASES

Simulation condition	Headway (s)	U_{oc}(V)
Case 1	150	836 to 880
Case 2	600	880 to 836
Case 3	150 to 450	836
Case 4	450 to 150	880

D. Fuzzy Rule of Discharge Control Module

The fuzzy rules of discharge control module shown in Table VI are relatively simple compared with charge control module. The proposed fuzzy rule needs to judge whether the no-load voltage is lower than the discharge voltage threshold U_{dis} and whether the discharge threshold is lower leading to the lower discharge energy of ESS.

E_{sc_out} is very low, the E_{sc_out} is increased by increasing U_{dis}. If the output energy of substation reduces and the discharge energy of the ESS increases, U_{dis} is promoted until E_{sc_out} and E_{sub} are no longer changed. When the discharge energy of the substation increases and the charge energy of the ESS changes a little, it is judged that the no-load voltage is lower than U_{dis}, and then U_{dis} should be reduced.

V. SIMULATION ANALYSIS

The ESS energy management strategy based on fuzzy control is simulated and verified by TPSS simulation platform. In the simulation conditions, the line parameters, train operation conditions and ESS configuration parameters are the same as above. Four different simulation environments are set up to verify the proposed strategy. Case 1 and case 2 analyze the adjustment process of charge/discharge voltage threshold under no-load voltage fluctuation, and case 3 and case 4 analyze the adjustment process of threshold under the change of headway. The simulation conditions are shown in Table VII.

In case 1 shown in Fig. 21(a) that the no-load voltage rises from 836 V to 880 V. At 0 s, U_{char} is 870 V. At 450 s, due to the

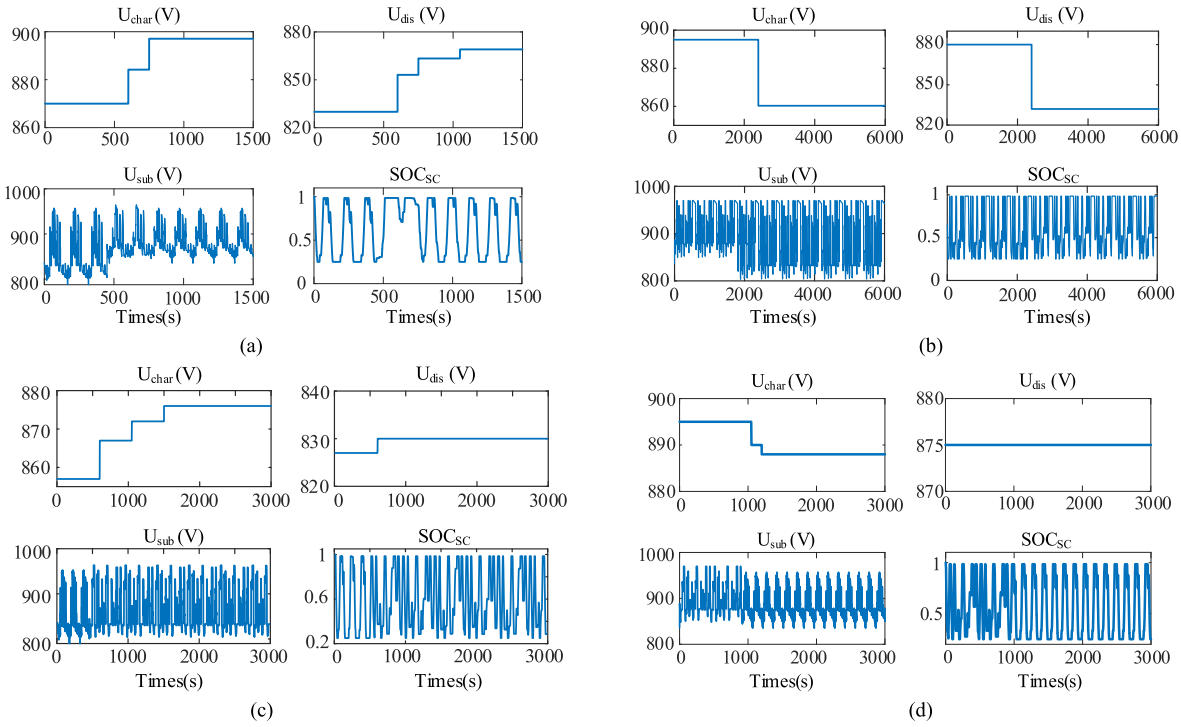

Fig. 21. The simulation results of U_{char}, U_{dis}, U_{sub} and SOC_{SC} (a) case 1, (b) case 2, (c) case 3, and (d) case 4.

increase of no-load voltage, the minimum voltage of the substation rises and U_{dis} is too low, so ESS cannot release energy. During 450 s to 600 s, E_{sub} increases, and the discharge/charge energy of ESS decrease, so the U_{char} and U_{dis} are increased accordingly at next period. The final U_{char} is 895 V and U_{dis} is 868 V.

In Fig. 21(b), the no-load voltage drops from 880 V to 836 V at 1800 s. U_{dis} is larger than the no-load voltage, which results in the increase of discharge /charge energy. This part of the increased energy is due to the increase of E_{sub}. To follow the no-load voltage, U_{char} is reduced from 895 V to 860 V, and U_{dis} is reduced from 880 V to 828 V.

In Fig. 21(c), while the headway changes from 150 s to 450 s at 450 s, E_{sub} has been greatly increased, while the charge energy and discharge energy of ESS increase correspondingly. At this point, the voltage fluctuation of substation decreases. In order to increase the energy interaction between trains, both U_{char} and U_{dis} are improved.

The simulation results of headway changes from 450 s to 150 s at 900 s are exhibited in Fig. 21(d), E_{sub}, E_{sc_in} and E_{sc_out} decrease correspondingly. Contrast with Case 3, the voltage fluctuation of the substation increases. U_{char} is lowered to reduce the on-board brake resistance to share regenerative braking energy.

J_1 and J_2 of the adaptive control strategy and the fixed threshold control strategy in the four cases are shown in Table VIII. It can be seen from the table that the regenerative braking energy utilization rate can be improved 5.37% by using the proposed strategy under the case1. The proposed strategy can improve the efficiency of regenerative energy utilization more obviously. In addition, the energy interaction rate is also slightly improved compared with the fixed threshold control strategy. Similarly, the proposed control strategy in Case2 have advantages over the fixed threshold control strategy. It can be seen from the comparison between Case1 and Case2 that inappropriate charge and discharge threshold has a greater impact on energy saving while no-load voltage increases. It is also found from Case3 and Case 4 that the proposed control strategy can not only have little impact on the energy saving rate, but also improve the energy interaction rate between trains while the headway changes, which demonstrates that the regenerative braking energy can be preferentially used by the traction train nearby.

TABLE VIII
EVALUATION INDEXES IN FOUR CASES

Simulation condition	J_1		J_2	
	Proposed strategy	Fixed threshold	Proposed strategy	Fixed threshold
Case 1	10.08%	4.71%	85.14%	84.98%
Case 2	29.77%	27.35%	38.13%	38.00%
Case 3	25.41%	24.20%	56.40%	54.10%
Case 4	16.41%	14.70%	73.21%	73.17%

VI. EXPERIMENTAL VERIFICATION

In order to verify the effectiveness of the proposed strategy, ground ESS is used to conduct an experimental test during the official operation of Beijing Subway Batong Line. ESS is installed in Liyuan Station (yellow pentagram in Fig. 22).The ground ESS experiment platform contains 6 cabinets, as shown in Fig. 22, including positive rail, negative cabinet, control cabinet, two SC cabinets and DC/DC converter cabinet. The SCs

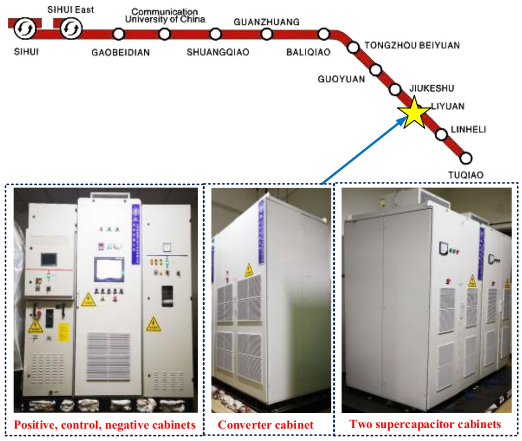

Fig. 22. Photos of the ground ESS installed in Liyuan substation.

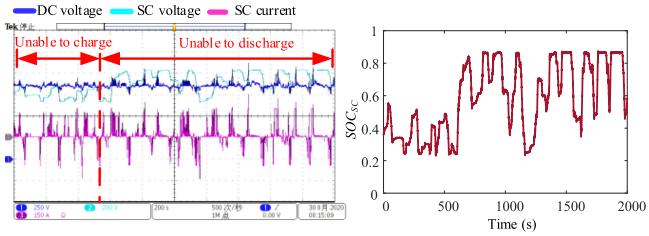

Fig. 23. Experiment waveform under fixed threshold.

use 48 V/165F modules produced by Maxwell, which has the same capacity as the configuration used in the simulation. The series and parallel number of SC modules in each SC cabinet is 14s4p.

The SC cabinets are connected in parallel with two DC-DC converters respectively. The converter cabinet is connected in parallel on the 750 V DC bus of substation. The control cabinet realizes the logic protection and energy management of the system. Positive and negative cabinets realize the input and exit of the experiment plat in the TPSS.

ESS has been put into use during the daily operation of the subway, the experiment waveform of proposed EMS is shown in Fig. 23 and Fig. 24. Operation waveform of ESS under fixed threshold was exhibited in Fig. 23. It can be seen that because the threshold cannot be adjusted adaptively according to the current ESS state, ESS would not be able to charge or discharge.

Fig. 24 shows the waveform of ESS operation during the short headway and long headway. In Fig. 24(a) the charge and discharge voltage threshold is adjusted for a cycle of about 120 s. It is clear that when ESS is in the state of poor charge and discharge in the first cycle, ESS can return to the condition of full charge and discharge after three cycles under the proposed adaptive EMS. Table IX shows the energy consumption of the ESS during each cycle in Fig. 24(a). According to this table, both the charge and discharge energy of ESS are gradually increasing and remain stable after the third cycle. During the first cycle, E_{sc_in} and E_{sc_out} are 0.95 kWh and 1.91 kWh respectively. At the last cycle, the ESS can reach 3.77 kWh in charge and 3.38 kWh in discharge. ESS charge energy increased

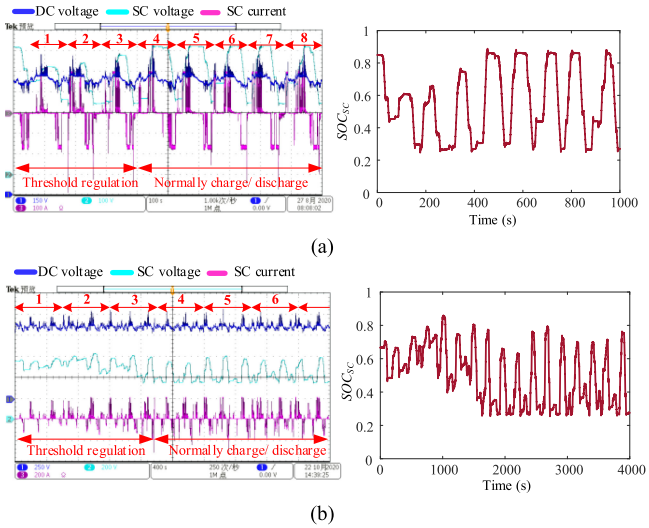

Fig. 24. Experiment waveform of proposed EMS (a) short headway and (b) long headway.

TABLE IX
ENERGY CONSUMPTION OF THE ESS IN SHORT HEADWAY

	E_{sc_in}(kWh)	E_{sc_out}(kWh)	E_{sub}(kWh)	U_{char}(V)	U_{dis}(V)
1	0.95	1.91	18.69	863	810
2	2.40	2.23	18.12	870	815
3	3.21	2.82	17.57	872	818
4	3.64	3.35	16.93	872	820
5	3.53	3.45	17.07	872	820
6	3.74	3.52	16.42	872	820
7	3.77	3.38	17.08	872	820
8	3.89	3.57	16.79	872	820

by up to 2.82kWh and substation output energy decreased by up to 1.61 kWh. The performance of the adaptive regulating ESS to recover regenerative braking energy can illustrate the effectiveness of the proposed strategy.

Fig. 24(b) shows the obtained outcomes with around 600 s as a cycle. According to Fig. 24(b), the charge energy and discharge energy of ESS is low, and the output energy of the substation is large in the first cycle. During the second and third cycles, the charge and discharge effects of ESS are improved. In the fourth cycle, ESS returns to normal charge/discharge state and remains stable in the following cycles. Table X presents the energy consumption of each cycle. From Table VIII, E_{sc_in} and E_{sc_out} are 5.62 kWh and 3.36 kWh respectively, while U_{char} and U_{dis} are 880 V and 838 V respectively, in the first cycle. At the end of the first cycle, the charge and discharge energy of ESS is detected to decrease, and the output energy of the substation increases. Therefore, the charge threshold is reduced and the discharge threshold is increased in the second cycle. When U_{char} and U_{dis} are 890 V and 850 V respectively, the charge and discharge energy of the ESS tends to be stable. There is 5.49 kWh charge energy more than the first cycle.

TABLE X
ENERGY CONSUMPTION OF THE ESS IN LONG HEADWAY

	E_{sc_in}(kWh)	E_{sc_out}(kWh)	E_{sub}(kWh)	U_{char}(V)	U_{dis}(V)
1	5.62	3.36	27.79	880	838
2	8.18	7.82	25.93	888	845
3	10.73	10.28	24.29	890	848
4	9.25	9.13	24.15	890	850
5	12.08	11.75	24.87	890	850
6	11.11	10.96	24.35	890	850

VII. CONCLUSION

This paper first analyzes the law of energy flow of the traction power supply system without energy storage system, and then extracts the law of energy distribution of the traction power supply system under different charge and discharge thresholds based on the traditional control strategy. On the premise of improving the recovery rate of regenerative energy, the ESS adaptive control strategy is proposed to ensure the energy interaction between trains. The strategy is divided into charging voltage threshold control and discharging voltage threshold control. The variation of the substation's output energy, the charge energy and discharge energy of the ESS and their variations are taken as inputs, and the charge voltage threshold and discharge voltage threshold of ESS are taken as outputs. At last, a ground ESS was used to verify the control strategy in Liyuan Station of Beijing Metro Batong Line. It can be seen from the experiment that the charge and discharge threshold of ESS can be well adjusted according to the change of energy. It ensures the recovery and utilization rate of the renewable energy in the ESS.

REFERENCES

[1] H. Hayashiya *et al.*, "Review of regenerative energy utilization in traction power supply system in Japan: Applications of energy storage systems in d.c. traction power supply system," in *Proc. 43rd Ann. Conf. IEEE Ind. Electron. Soc.*, 2017, pp. 3918–3923.

[2] A. Gonzalez-Gil, R. Palacin, and P. Batty, "Sustainable urban rail systems: Strategies and technologies for optimal management of regenerative braking energy," *Energy Convers. Manage.*, vol. 75, no. 5, pp. 374–388, Nov. 2013.

[3] A. Gonzalez-Gil *et al.*, "A systems approach to reduce urban rail energy consumption," *Energy Convers. Manage.*, vol. 80, pp. 509–524, Apr. 2014.

[4] M. Khodaparastan, A. A. Mohamed, and W. Brandauer, "Recuperation of regenerative braking energy in electric rail transit systems," *IEEE Trans. Intell. Transp. Syst.*, vol. 20, no. 8, pp. 2831–2847, Aug. 2019.

[5] D. Ramsey, T. Letrouve, A. Bouscayrol, and P. Delarue, "Comparison of energy recovery solutions on a suburban DC railway system," *IEEE Trans. Transp. Elect.*, vol. 7, no. 3, pp. 1849–1857, Sep. 2021.

[6] T. Ratniyomchai, S. Hillmansen, and P. Tricoli, "Recent developments and applications of energy storage devices in electrified railways," *IET Elect. Syst. Transp.*, vol. 4, no. 1, pp. 9–20, Mar. 2014.

[7] M. Khodaparastan, O. Dutta, M. Saleh, and A. A. Mohamed, "Modeling and simulation of DC electric rail transit systems with wayside energy storage," *IEEE Trans. Veh. Technol.*, vol. 68, no. 3, pp. 2218–2228, Mar. 2019.

[8] Q. Qin, T. Guo, F. Lin, and Z. Yang, "Energy transfer strategy for urban rail transit battery energy storage system to reduce peak power of traction substation," *IEEE Trans. Veh. Technol.*, vol. 68, no. 12, pp. 11714–11724, Dec. 2019.

[9] F. Ciccarelli, D. Iannuzzi, K. Kondo, and L. Fratelli, "Line-voltage control based on wayside energy storage systems for tramway networks," *IEEE Trans. Power Electron.*, vol. 31, no. 1, pp. 884–899, Jan. 2016.

[10] Z. Gao, J. Fang, Y. Zhang, and D. Sun, "Control strategy for wayside supercapacitor energy storage system in railway transit network," *J. Modern Power Syst. Clean Energy*, vol. 2, no. 2, pp. 181–190, Jun. 2014.

[11] J. Wang *et al.*, "Thresholds modification strategy of wayside supercapacitor storage considering DC substation characteristics," in *Proc. 41st Annu. Conf. IEEE Ind. Elect. Soc.*, 2015, pp. 002076–002081.

[12] H. Hayashiya *et al.*, "Proposal of a novel control method of Li-ion battery system for regenerative energy utilization in traction power supply system," in *Proc. 2016 IEEE Int. Power Electron. Motion Control Conf.*, 2016, pp. 298–303.

[13] F. Zhu, Z. Yang, F. Lin, and Y. Xin, "Dynamic threshold adjustment strategy of supercapacitor energy storage system based on no-load voltage identification in urban rail transit," in *Proc.2019 IEEE Transp. Elect. Conf. Expo, Asia-Pacific*, 2019, pp. 1–6.

[14] P. J. Grbovic, P. Delarue, P. Le Moigne, and P. Bartholomeus, "Modeling and control of the ultracapacitor-based regenerative controlled electric drives," *IEEE Trans. Ind. Electron.*, vol. 58, no. 8, pp. 3471–3484, Aug. 2011.

[15] A. Castaings, H. Caron, H. Kharrat, A. Ovalle, and B. Vulturescu, "Energy storage system based on supercapacitors for a 750 v DC railway power supply," in *Prof. 2018 IEEE Int. Conf. Elect. Syst. Aircr., Railway, Ship Propuls. Road Veh. Int. Transp. Elect. Conf.*, 2018, pp. 1–5.

[16] F. Ciccarelli, A. Del Pizzo, and D. Iannuzzi, "Improvement of energy efficiency in light railway vehicles based on power management control of wayside lithium-ion capacitor storage," *IEEE Trans. Power Elect.*, vol. 29, no. 1, pp. 275–286, Jan. 2014.

[17] F. Ciccarelli and D. Iannuzzi, "A novel energy management control of wayside li-ion capacitors-based energy storage for urban mass transit systems," in *Proc Int. Symp. Power Electron. Power Electron., Elect. Drives, Automat. Motion*, 2012, pp. 773–779.

[18] F. Ciccarelli, D. Iannuzzi, D. Lauria, and P. Natale, "Optimal control of stationary lithium-ion capacitor-based storage device for light electrical transportation network," *IEEE Trans. Transp. Elect.*, vol. 3, no. 3, pp. 618–631, Sep. 2017.

[19] Z. Yang, Z. Yang, H. Xia, and F. Lin, "Brake voltage following control of supercapacitor-based energy storage systems in metro considering train operation state," *IEEE Trans. Ind. Electron.*, vol. 65, no. 8, pp. 6751–6761, Aug. 2018.

[20] R. Barrero, X. Tackoen, and J. van Mierlo, "Stationary or onboard energy storage systems for energy consumption reduction in a metro network," in *Proc. Inst. Mech. Engineers, Part F: J. Rail Rapid Transit*, vol. 224, no. 3, pp. 207–225, 2010.

[21] X. Chen, Y. Wang, and Q. Wu, "A bio-fuel power generation system with hybrid energy storage under a dynamic programming operation strategy," *IEEE Access*, vol. 7, pp. 64966–64977, 2019.

[22] F. Zhu, Z. Yang, F. Lin, and H. Xia, "Scene-segmentation based control strategy of energy storage system for urban railway," in *Proc 2017 IEEE 20th Int. Conf. Intell. Transp. Syst.*, 2017, pp. 1–7.

[23] H. Kobayashi, K. Kondo, and D. Iannuzzi, "A theoretical analysis on dynamic and static characteristics of control strategies for wayside energy storage system in DC-electrified railway," in *Proc 2018 IEEE Int. Conf. Elect. Syst. Aircr., Railway, Ship Propul. Road Veh. Int. Transp. Elect. Conf.*, 2018, pp. 1–6.

[24] Z. Yang, F. Zhu, and F. Lin, "Deep-reinforcement-learning-based energy management strategy for supercapacitor energy storage systems in urban rail transit," *IEEE Trans. Intell. Transp. Syst.*, vol. 22, no. 2, pp. 1–11, Jan. 2020.

[25] F. Zhu, Z. Yang, F. Lin, and Y. Xin, "Decentralized cooperative control of multiple energy storage systems in urban railway based on multiagent deep reinforcement learning," *IEEE Trans. Power Electron.*, vol. 35, no. 9, pp. 9368–9379, Sep. 2020.

[26] Y. Yoshida, S. Arai, H. Kobayashi, and K. Kondo, "Charge/discharge control of wayside batteries via reinforcement learning for energy-conservation in electrified railway systems," *Elect. Eng. Jpn.*, vol. 214, pp. e23319, 2021.

[27] H. Yu, D. Tarsitano, X. Hu, and F. Cheli, "Real time energy management strategy for a fast charging electric urban bus powered by hybrid energy storage system," *Energy*, vol. 112, pp. 322–331, Oct. 2016.

[28] F. Peng *et al.*, "Development of master-slave energy management strategy based on fuzzy logic hysteresis state machine and differential power processing compensation for a PEMFC-LIB-SC hybrid tramway," *Appl. Energy*, vol. 206, pp. 346–363, Nov. 2017.

[29] J. Chen, C. Xu, C. Wu, and W. Xu, "Adaptive fuzzy logic control of fuel-cell-battery hybrid systems for electric vehicles," *IEEE Trans. Ind. Informat.*, vol. 14, no. 1, pp. 292–300, Jan. 2018.

[30] H. Yin, W. Zhou, M. Li, C. Ma, and C. Zhao, "An adaptive fuzzy logic-based energy management strategy on battery/ultracapacitor hybrid electric vehicles," *IEEE Trans. Transp. Elect.*, vol. 2, no. 3, pp. 300–311, Sep. 2016.
[31] Y. Zhang, C. Zhang, Z. Huang, L. Xu, Z. Liu, and M. Liu, "Real-Time energy management strategy for fuel cell range extender vehicles based on nonlinear control," *IEEE Trans. Transp. Elect.*, vol. 5, no. 4, pp. 1294–1305, Dec. 2019.
[32] M. Kandidayeni, A. O. M. Fernandez, A. Khalatbarisoltani, L. Boulon, S. Kelouwani, and H. Chaoui, "An online energy management strategy for a fuel cell/battery vehicle considering the driving pattern and performance drift impacts," *IEEE Trans. Veh. Technol.*, vol. 68, no. 12, pp. 11427–11438, Dec. 2019.
[33] H. Tian, X. Wang, Z. Lu, Y. Huang, and G. Tian, "Adaptive fuzzy logic energy management strategy based on reasonable SoC reference curve for online control of plug-in hybrid electric city bus," *IEEE Trans. Intell. Transp. Syst.*, vol. 19, no. 5, pp. 1607–1617, May 2018.

Yuyan Liu (Student Member, IEEE) received the B.S. and M.S. degrees in 2015 and 2017, respectively, in electrical engineering from Beijing Jiaotong University, Beijing, China, where she is currently working toward the Ph.D. degree with the School of Electrical Engineering. Her research interests include energy management of energy storage systems and optimal operation of multiple trains in urban rail transit.

Zhongping Yang (Member, IEEE) received the B.Eng. degree in electrical engineering from the Tokyo University of Mercantile Marine, Tokyo, Japan, in 1997, and the M.Eng. and Ph.D. degrees in electrical engineering from the University of Tokyo, Tokyo, Japan, in 1999 and 2002, respectively. He is currently a Professor with the School of Electrical Engineering, Beijing Jiaotong University, Beijing, China. His research interests include high-speed rail integration technology, traction and regenerative braking technology, and wireless power transfer of urban rail vehicles.

Xiaobo Wu (Member, IEEE) received the B.S. and M.S. degrees from the China University of Petroleum, Qingdao, China, in 2011 and 2014, respectively. From 2014 to 2019, he was an Electrical Engineer with CNPC East China Design Institute Company, Ltd, engaged in power supply system design. He is currently an Engineer with the National Innovation Center of High Speed Train, Qingdao, China. His research interests include optimization of energy and power system, energy efficiency of traction power supply system.

Lifu Lan (Student Member, IEEE) received the M.S. degree in 2017 in electrical engineering from Beijing Jiaotong University, Beijing, China, where he is currently working toward the B.S. degree with the School of Electrical Engineering. His research interests include soft switching technology in the field of DC-DC converters and application of high-power DC-DC converter in the field of energy storage.

Fei Lin (Member, IEEE) received the B.S. degree in electrical engineering from Xi'an Jiaotong University, Xi'an, China, in 1997, the M.S. degree in electrical engineering from Shandong University, Jinan, China, in 2000, and the Ph.D. degree in electrical engineering from Tsinghua University, Beijing, China, in 2004. He is currently a Professor with the School of Electrical Engineering, Beijing Jiaotong University, Beijing, China. His research interests include traction converters and motor drives, energy management for railway systems, and digital control of power-electronic-based devices.

Hu Sun (Member, IEEE) received the B.S. and M.S. degrees from North China Electric Power University, Baoding, China. He is currently a Senior Engineer with the Institute of Power Electronics, School of Electrical Engineering, Beijing Jiaotong University, Beijing, China. His current research interests include technical research on electric traction AC drive mutual feed test control system and converter detection test system.

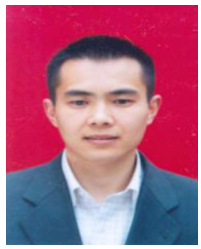

Jiangbo Huang (Member, IEEE) received the M.S. degree from Chongqing University, Chongqing, China. He is currently a M.S. tutor with the School of Robot Engineering, Yangtze Normal University, Chongqing, China. His research interests include design and intelligent control of power electronic converter.